OCT structure, COB location and magmatic type of the Northern Angolan margin from integrated quantitative analysis of deep seismic reflection and gravity anomaly data

L Cowie[1], R.M Angelo[1, 2], N Kusznir[1], G Manatschal[3] and B Horn[4]

[1] Earth and Ocean Sciences, University of Liverpool, Liverpool, L69 3BX, UK

[2] Presently at ConocoPhillips, Houston, TX 77079, USA

[3] CNRS-EOST, Université de Strasbourg, 1 rue Blessing, F-67084 Strasbourg, France

[4] ION Geophysical / GX Technologies, Houston, Texas, USA

Abstract

The crustal structure and distribution of crustal type of the northern Angolan rifted continental margin are greatly debated; hyper-extended continental crust, oceanic crust and exhumed serpentinised mantle have been proposed to underlie the Aptian salt and the underlying sag sequence. Quantitative analysis of deep seismic reflection and gravity anomaly data together with reverse post-breakup subsidence modelling has been used to investigate ocean-continent transition structure, continent-ocean boundary location, crustal type and the palaeo-bathymetry of Aptian salt deposition. Gravity inversion to give Moho depth and crustal thickness, RDA analysis to identify departures from oceanic bathymetry and subsidence analysis shows that the distal Aptian salt is underlain by hyper-extended continental crust rather than exhumed mantle or oceanic crust. We propose that Aptian salt was deposited approximately 0.2km and 0.6km below global sea level and that the inner proximal salt subsided by post-rift (post-tectonic) thermal subsidence alone, while the

outer distal salt formed during syn-rift, prior to breakup, resulting in additional tectonic subsidence. Our analysis argues against Aptian salt deposition on the Angolan margin in a 2-3km deep isolated ocean basin, and supports salt deposition on hyper-extended continental crust formed by diachronous rifting migrating from east to west, culminating in late Aptian.

1. Introduction

The northern Angolan rifted continental margin has been the subject of extensive seismic surveys (e.g. Contrucci et al. (2004), Moulin et al. (2005) and Unternehr et al.(2010)). Seismic imaging and interpretation of the sub-salt is difficult due to the presence of thick sedimentary packages which are impacted by a massive middle to upper Aptian salt sequence (up to 5km thickness in places); this presents major scientific and technical challenges to understanding crustal structure and tectonic history. As a result the ocean-continent transition (OCT) structure and continent-ocean boundary (COB) location along the northern Angolan margin are still not fully understood. The presence and distribution of thinned continental crust, oceanic crust and exhumed mantle, the nature of the pre-salt sag basins, the tectonic context of the Aptian salt deposition and whether the salt is pre-breakup or post-breakup, the palaeo-water depths through the breakup period and the mechanisms responsible for the generation of accommodation space are uncertain and much debated (Jackson et al., 2000; Karner and Driscoll, 1999; Karner et al., 2003; Karner et al., 1997; Moulin, 2003; Moulin et al., 2005). In particular there is controversy about whether the salt was deposited in a deep isolated ocean basin or on thinned continental crust.

Our analysis along the offshore northern Angolan margin is focussed along three profiles in the Kwanza region; locations are indicated in Figure 1(a). The three profiles include the ION deep long offset seismic reflection profile CS1-2400 (Figure 1(c)), the P3 (Figure 1(d)) and P7+11 profiles (Figure 1(e)) (Contrucci et al., 2004; Moulin et al., 2005). The aims of this paper are to determine the OCT structure along the northern Angolan rifted continental margin, to provide an understanding of the

palaeo-bathymetries of both proximal and distal base Aptian salt deposition and to examine the location of the salt within the broad framework of the OCT.

2. Integrated Quantitative Analysis Methodology

Integrated quantitative analysis of deep seismic reflection and gravity anomaly data has been applied to the Kwanza margin, offshore northern Angola, in order to determine OCT structure, COB location and magmatic type using ION deep long-offset seismic reflection data. The integrated work-flow and quantitative analytical techniques, which have been applied, consist of: gravity anomaly inversion, residual depth anomaly (RDA) analysis and subsidence analysis. The combined interpretation of these independent quantitative measurements is used to determine OCT structure, COB location and margin magmatic type. This integrated approach has been validated on the Iberian margin (Cowie, 2015) where ODP drilling provides ground-truth of OCT crustal structure, COB location and magmatic type. In addition, we apply a joint inversion technique, using deep seismic reflection and gravity anomaly data, to determine the lateral variation of crustal basement density and seismic velocity for the ION deep seismic reflection profile CS1-2400. The joint inversion of deep seismic and gravity data provides validation of crustal basement thickness interpreted from deep long-offset seismic reflection data and is used to help further constrain crustal basement type.

2.1. Crustal basement thickness and continental lithosphere thinning from gravity anomaly inversion

Gravity anomaly inversion has been used to determine Moho depth, crustal basement thickness, and continental lithosphere thinning factors (1- 1/β). The data used within our gravity anomaly inversion are bathymetry (Amante and Eakins, 2009) (Figure 1(a)), satellite derived free air gravity (Sandwell and Smith, 2009) (Figure 1(b)), 2D sediment thickness from pre-stacked depth migrated (PSDM) seismic reflection data along CS1-2400 profile (Figure 1(c)) and ocean age isochrons from Müller et al. (1997). The gravity anomaly inversion methodology is described in Chappell and Kusznir (2008)

71 and Greenhalgh and Kusznir (2007) and has been applied in Cowie and Kusznir (2012) and Alvey et
72 al. (2008).

73 The gravity anomaly inversion method is carried out in the 3D spectral domain, using the scheme of
74 Parker (1972) and also incorporates a lithosphere thermal gravity anomaly correction, which
75 accounts for the lithosphere mass deficiency due to the elevated geothermal gradient within
76 oceanic and thinned continental margin lithosphere. Without the inclusion of the lithosphere
77 thermal gravity anomaly correction at rifted continental margins, predicted Moho depth and crustal
78 basement thickness are too thick and continental lithosphere thinning factors are too low. The
79 thermal gravity anomaly correction is dependent on the thermal re-equilibration time since
80 lithosphere stretching and thinning, and therefore on continental breakup age. There is general
81 agreement (e.g. Karner and Gambôa (2007) and Aslanian et al.(2009)) that rifting on the Angolan
82 margin started in the Neocomian and culminated with continental breakup in the late Aptian.
83 However, there is no consensus on the rates of lithosphere stretching and thinning through this time
84 interval, although there is some evidence that deformation rates accelerated in the Barremian and
85 Aptian (e.g. Crosby et al. (2011)). While a finite rifting model would be appropriate to determine the
86 lithosphere thermal anomaly developed during lithosphere stretching and thinning leading to
87 breakup, the history of rifting rates is not known. As a consequence we use an instantaneous rift
88 model to determine lithosphere thermal perturbation and explore upper and lower bounds of rift
89 age. We have used 112Ma, corresponding to the age of breakup, after Moulin (2005), for the
90 preferred thermal re-equilibration time to determine the lithosphere thermal gravity anomaly
91 correction, but have also examined sensitivities to ages for thermal re-equilibration which span the
92 period Berriasian (140Ma) to early Albian (110Ma). This range corresponds to the start and end of
93 the main rifting episode in the South Atlantic (Teisserenc and Villemin, 1989).

94 Gravity anomaly inversion Moho depths have been calibrated against seismic Moho depths from the
95 oceanic domain of the CS1-2400 profile using the clear Moho reflectors. Calibration suggests that a

reference Moho depth of 35.5km is required in order to predict crustal basement thicknesses consistent with those seen in the oceanic domain of the CS1-2400 seismic reflection profile. An uncertainty in the oceanic Moho depth on the CS1-2400 PSDM depth section, used for the calibration of reference Moho depth, arises from uncertainty in basement seismic velocity but is estimated to be no more than +/- 0.5km.

A crustal cross section along the CS1-2400 profile (Figure 2(a)) has been constructed using Moho depths predicted from gravity anomaly inversion assuming the calibrated reference Moho depth of 35.5km; bathymetry and 2D sediment thickness are from the CS1-2400 seismic profile. The crustal cross section highlights changes in crustal basement thicknesses along the CS1-2400 profile. At the western end of the profile the gravity anomaly inversion predicts crustal basement thicknesses between 5km and 7km; in the central region of the profile crustal basement thicknesses thicken to approximately 11km and at the eastern end of the profile the crustal basement thickens to approximately 25km. Moho depths determined from the gravity anomaly inversion are generally in good agreement with those seen on the CS1-2400 seismic profile.

The corresponding continental lithosphere thinning factor ($\gamma=1-1/\beta$) estimates for profile CS1-2400, derived from gravity anomaly inversion, assuming depth uniform stretching and thinning are shown in Figure 2(b). Continental lithosphere thinning factors of zero indicate that there has been no stretching or thinning of the continental lithosphere, whereas a continental lithosphere thinning factor of one indicates that there has been infinite stretching and thinning of the original continental lithosphere and that no continental crust or lithosphere remains. Stretching of continental lithosphere leads to a decrease in crustal basement thickness; however, decompression melting during rifting and seafloor spreading generates oceanic crust, SDRS (seaward dipping reflectors) and magmatic underplating, which increases crustal basement thickness. A correction for magmatic addition has been included within the gravity anomaly inversion method, and uses a parameterization of the decompression melting model of White and McKenzie (1989) to predict the

thickness of the crustal magmatic addition (see Chappell & Kusznir (2008)). Decompression melting and the resulting volume and timing of magmatism during rifting and continental breakup is sensitive to the thermal structure of the continental lithospheric and asthenospheric mantle, its chemical composition (enriched or depleted), the rate of lithosphere stretching and thinning, and the amount of melt retention within the mantle. As a consequence we do not believe that it is possible to apply a deterministic approach to the prediction of magmatic addition. Instead we examine two end members; normal magmatic addition and magma-starved. A 'normal' magmatic solution corresponds to 'normal' decompressional melting that predicts a 7km thick oceanic crust, which is initiated at a critical thinning factor of 0.7. In our magma-starved solution, there is no magmatic addition from decompression melting.

The distribution of continental lithosphere thinning factors can be used to help constrain OCT structure and COB location along the profile. At the western end of the profile the continental lithosphere thinning factors for a 'normal' magmatic solution are 1.0 whilst for a magma-starved solution the continental lithosphere thinning factors are approximately 0.85. In the central section of the profile, the continental lithosphere thinning factors, for both solutions examined, reduce to between 0.7 and 0.85. At the western end of the profile we prefer the normal magmatic solution; however, in the central and eastern region of the profile we believe that the magma-starved solution is preferential.

Using an older age of 140Ma for the age of lithosphere thermal perturbation (and thermal relaxation) reduces the magnitude of the lithosphere thermal gravity anomaly correction. As a consequence this gives a slightly deeper Moho, thicker crust and lower thinning factors for the central and eastern part of the profile. This sensitivity to rift age is relatively minor and does not affect the interpretation of OCT structure or crustal type.

2.2. Residual depth anomaly (RDA) analysis along the CS1-2400 profile

RDA analysis has been applied to examine OCT bathymetric anomalies with respect to expected oceanic bathymetries along the CS1-2400 profile (Figure 3). RDAs are commonly used for oceanic regions to compare observed bathymetry with that predicted from secular cooling models of oceanic lithosphere. A RDA, for oceanic crust, is the difference between observed bathymetry (b_{obs}) and bathymetry predicted from ocean age ($b_{predicted}$).

$$RDA = b_{obs} - b_{predicted} \quad (1)$$

Zero oceanic RDAs correspond to oceanic crust of global average thickness (7 km) in the absence of mantle dynamic topography; positive RDAs correspond to thicker than average oceanic crust, and negative RDAs to thin oceanic crust or serpentinised exhumed mantle. We determine RDAs for the CS1-2400 profile in order to investigate where the RDA signal varies from that seen in the oceanic domain due to changes in crustal thickness and composition across the ocean-continent transition. The age of the lithosphere thermal perturbation due to rifting and breakup in the ocean-continent transition, and its thermal re-equilibration time, correspond to the breakup age and the age of the oldest oceanic lithosphere.

Age predicted bathymetric anomalies have been calculated from Crosby and McKenzie (2009). The age of oceanic lithosphere is taken from the global ocean isochron model of Müller et al. (2008). The region inboard of the oldest ocean isochron (corresponding to the breakup age) may be given that age or the isochron gradient may be projected into the margin. The difference in the predicted RDA between these two approaches to defining the thermal age of the continental margin lithosphere is negligible and has no impact on the RDA interpretation. Sensitivities to the thermal plate model predictions from Parsons and Sclater (1977) and Stein and Stein (1992) have also been examined; RDA results computed using these different thermal plate model predictions do not differ significantly.

RDAs have been corrected for sediment loading. Present day bathymetry is corrected for sediment loading using flexural backstripping and decompaction (Kusznir et al., 1995) which comprises the removal of the sedimentary load, allowing for the flexural isostatic response and decompaction of the remaining sediments. Flexural backstripping and decompaction assumes shaly-sand compaction and density (Sclater and Christie, 1980) during the removal of the sedimentary layer, whilst the salt layer is given a simple salt lithology (Hudec and Jackson, 2007). Figure 3(b) shows a comparison of the uncorrected RDA and the sediment corrected RDA along the CS1-2400 profile (Figure 3(a)). At the western end of the profile there is approximately a 1500m difference between the uncorrected RDA and the sediment corrected RDA, the largest difference is seen in the central section of the profile. The sediment corrected RDA along the CS1-2400 profile (Figure 3(b)), is positive with a magnitude between zero and +300m at the western end of the profile.

The sediment corrected RDA has a minor sensitivity to the effective elastic thickness used during flexural backstripping to define flexural isostatic response to the sediment unloading correction. We use an effective elastic thickness of 1.5km which is appropriate for the shorter wavelength syn-rift sediment loads (see Roberts et al. (1998) for further discussion).

2.3. Continental lithosphere thinning from subsidence analysis along the CS1-2400 profile

Subsidence analysis has been used to determine the distribution of continental lithosphere thinning and the distal extent of continental crust in order to constrain OCT structure. Subsidence analysis involves the conversion of water loaded subsidence into continental lithosphere thinning factors, assuming McKenzie (1978). Water loaded subsidence, determined by flexural backstripping, is interpreted as the sum of initial (Si) and thermal (St) subsidence in the context of the McKenzie (1978) intra-continental rift model. A correction for magmatic addition due to adiabatic decompression (White and McKenzie, 1989) during continental rifting and seafloor spreading has been included (see Roberts et al. (2013)) and uses the same scheme as described earlier in the

gravity anomaly inversion methodology. Magmatic addition from decompression melting increases the thickness of the crust thinned by lithosphere stretching due to intrusion and extrusion, which isostatically reduces the initial subsidence as predicted by McKenzie (1978) and corresponds to the formation of oceanic crust.

Figure 4(b) shows sensitivities to continental lithosphere thinning factors from subsidence analysis, including a 'normal' magmatic solution, and a magma-starved solution, with reference to the CS1-2400 profile (Figure 4(a)). At the western end of the profile a 'normal' magmatic solution predicts thinning factors of 1.0 whilst a magma-starved solution predicts thinning factors of approximately 0.9.

2.4. Joint inversion of deep seismic and gravity anomaly data: application to the CS1-2400 profile

Joint inversion of deep seismic reflection and gravity anomaly data has been applied to the CS1-2400 profile in order to both (i) validate the seismic interpretation of Moho and to (ii) determine the lateral variation in crustal basement density and seismic velocity. The ION deep seismic profile has been interpreted in both the time (PSTM) and depth (PSDM) domain. The joint inversion process requires that the seismic reflection data shows seismic reflectivity from the Moho; for the CS1-2400 profile this corresponds to most of the section apart from beneath the thick distal salt.

Moho depth is first determined from gravity inversion, as described in section 2, using sediment thicknesses from the PSDM depth section.. The crustal basement thickness determined from gravity inversion is converted to interval two-way travel time and then added to the seismic interpretation of top basement on the PSTM time section to show the gravity Moho in the time domain. The basement seismic velocity V_p used for this conversion from interval depth to interval two-way travel time is calculated from the crustal basement density used in the gravity inversion using the empirical linear relationship proposed by Birch (Birch, 1964; Ludwig et al., 1970). The initial value of basement density used in the gravity inversion is 2850 kgm^{-3} (Chappell and Kusznir, 2008). Because the

comparison of the gravity Moho depth with the seismic reflection image is carried out in the time domain, the joint inversion methodology is not affected by uncertainties in the basement seismic velocities used to produce the PSDM depth seismic image.

The gravity inversion Moho for CS1-2400, converted into the time domain, is shown in Figure 5(a) superimposed on the PSTM section. The seismic interpretation of Moho two-way travel time and the gravity Moho depth taken into the time domain compare well. This suggests that the seismic interpretation of Moho on the PSTM section is correct and validates the deep seismic interpretation.

The differences in two-way travel time between the seismic and gravity Mohos is assumed to arise from heterogeneity in crustal basement density and seismic velocity. The joint inversion solves for coincident seismic and gravity Moho in the time domain and calculates the lateral variation of crustal basement density and seismic velocity along profile (Figure 5(c) & (d)). The joint inversion is carried out using the time domain (PSTM) seismic reflection data, as this is the raw data and does not have the assumed basement seismic velocities of the depth domain (PSDM) seismic sections.

Joint inversion determines the combination of basement seismic velocities and densities required, along the profile, in order to match the Moho predicted from gravity anomaly inversion to the picked Moho, in the time domain. Basement density and seismic velocity are assumed to be linked by Birch's empirical relationship (Birch, 1964). During the joint inversion, changes in basement density change the Moho predicted from gravity anomaly inversion in the depth domain; corresponding changes in seismic velocity change the conversion of the new gravity Moho from the depth domain into the time domain.

Basement densities and seismic velocities from the joint inversion, shown in Figure 5(c and d), show lateral variations along profile. The basement densities and seismic velocities for the western distal end of the CS1-2400 profile are significantly higher than those for the remaining profile. We suggest that the higher values in the west correspond to oceanic crustal basement while the lower values in

242 the centre and east correspond to continental crustal basement. The short wavelength variations in
243 basement density and seismic velocity arise from the inversion methodology and result from fault
244 controlled top basement topography.

245 Solving for the coincident seismic and gravity anomaly inversion predicted Moho in the time domain
246 gives an improved estimate of Moho depth. This improved estimate from joint inversion is shown in
247 Figure 5(b) and compared with that derived from gravity inversion alone.

248 3. OCT structure and COB location along the CS1-2400 profile

249 Within the literature there are a range of different definitions of the OCT and COB (e.g. Péron-
250 Pinvidic et al. (2007), Whitmarsh and Miles (1995), Manatschal et al. (2001), Dean et al. (2000)
251 Manatschal et al. (2010) and Discovery 215 Working Group (1998). Within this paper, we define the
252 OCT as the region between unequivocal continental crust of 'normal' thickness and unequivocal
253 oceanic crust; the lithosphere in this region is highly thinned, with complex tectonics, variable
254 magmatism and possible mantle exhumation. We define the COB as the distal limit of unequivocal
255 continental crust; however, determining the location of the COB is made difficult by the presence of
256 exhumed mantle and complex tectonics.

257 A composite analysis plot for profile CS1-2400 is shown in Figure 6, consisting of (a) crustal cross
258 section from gravity anomaly inversion, (b) comparison of the sediment corrected RDA and the RDA
259 component from crustal thickness variations (RDA_{CT}), (c) comparison of the continental lithosphere
260 thinning factors predicted from gravity anomaly inversion and subsidence analysis (d) lateral
261 variations in basement density and (e) seismic velocity from joint inversion. The joint inversion
262 results, including Moho depth, crustal basement densities and seismic velocities have been
263 'smoothed' by computing a moving average, using a spatial gate of 30km.

264 Due to the thick sedimentary cover and mobile salt (including salt diapirs and canopies), seismic
265 imaging of the salt and pre-salt sedimentary units is difficult, which could lead to errors in our

interpretation of the internal structure and thickness of the salt and the pre-salt sedimentary layers. We are however, more confident in our pick of the base salt. In order to understand the implications of either over or under estimating the thickness of the salt layer we have examined the effect of treating the salt layer as a sedimentary layer with a shaly sand lithology within the gravity inversion; this results in a slightly deeper Moho and smaller continental lithosphere thinning factors from the gravity inversion. The inclusion or omission of the salt layer does not fundamentally change our interpretation of the crustal domains along the profile.

The composite analysis plot is interpreted as showing three distinct crustal zones along the CS1-2400 profile highlighted by the dashed lines: zone A – oceanic crust, zone B – hyper-extended continental crust and zone C – continental crust. The dashed lines indicate the boundaries between each of these interpreted crustal domains; although these interfaces are shown as a sharp line, in reality they are likely to be transitional boundaries. The COB is identified as the ocean-ward start of 'normal' oceanic crust and is identified by changes in crustal basement thickness, inflections in the RDA analysis signals and also changes in the continental lithosphere thinning from subsidence analysis and gravity anomaly inversion.

Zone A - Oceanic crust

In zone A, the crustal basement thicknesses (Figure 6(a)) predicted from gravity anomaly inversion range between 5km and 6km, as expected for oceanic crust. Oceanic crust of normal thickness should have a sediment corrected RDA of approximately zero, notwithstanding the contribution of mantle dynamic topography. The sediment corrected RDA in this domain (Figure 6(b)) is slightly positive, consistent with the presence of oceanic crust together with some mantle dynamic uplift; this is in agreement with the mantle dynamic uplift reported by Crosby & McKenzie (2009) for the Angolan margin. In addition to the RDA corrected for sediment loading, the RDA component from variations in crustal basement thickness (RDA_{CT}) has also been computed, which is the result of the

presence of anomalously thick or thin crust. In this domain the RDA_{CT} is negative, which implies that the crustal basement is thinner than 7km, which is in agreement with the crustal basement thicknesses predicted from gravity inversion. The continental lithosphere thinning factors predicted from gravity anomaly inversion and subsidence analysis are in good agreement (Figure 6(c)) and predict continental lithosphere thinning factors of 1.0, for a 'normal' magmatic solution, implying the presence of oceanic crust. Joint inversion of deep seismic and gravity data calculates crustal basement densities for zone A which range between 2850kgm^{-3} and 3035kgm^{-3} (with an average basement density of approximately 2940kgm^{-3}) (Figure 6(d)) and seismic velocities, which range between 6.7kms^{-1} and 7.1kms^{-1} (Figure 6(e)). These basement densities (and corresponding seismic velocities) are larger than the crustal basement density (2850kgm^{-3}) used within the initial gravity anomaly inversion, which is to be expected as typical oceanic crustal densities range between 2860kgm^{-3} and 2900kgm^{-3} (Carlson and Herrick, 1990; Carlson and Raskin, 1984; Fowler, 2006).

Between the oceanic domain and the hyper-extended continental crust domain, we interpret a domain of transitional crust; we believe that the crust is a mix of hyper-extended continental crust and magmatic addition. We interpret the edges of this transitional region as the inner and outer bounds of the COB. Within this region we see an increase in crustal basement thickness and both the sediment corrected RDA and the RDA_{CT}, whilst the continental lithosphere thinning factors decrease. At the western end of the hyper-extended continental crust domain, the thinning of the continental crust may increase together with the start of magmatic addition as ocean crust is approached. Our interpretation of the presence of hyper-extended continental crust with the presence of magmatics in this region is significantly different to that proposed by Unternehr et al. (2010), who proposes the presence of serpentinized exhumed mantle. Our quantitative analysis results show no evidence of exhumed mantle; exhumed mantle would show a thinner crust from gravity inversion, negative sediment corrected RDAs and higher continental lithosphere thinning factors.

315 *Zone B - Hyper-extended continental crust*

316 In our interpreted hyper-extended continental crust domain, gravity anomaly inversion predicted
317 crustal basement thicknesses range between 7km and 12km (Figure 6(a)). Both the sediment
318 corrected RDA and the RDA_{CT} (Figure 6(b)) plateau in this domain, at approximately 1000m for the
319 sediment corrected RDA and at approximately 500m for the RDA_{CT}. The continental lithosphere
320 thinning factors from gravity anomaly inversion and subsidence analysis are in good agreement in
321 zone B (Figure 6(c)) and range between 0.7 and 0.85, which is indicative of thinned continental crust.
322 Basement densities and seismic velocities, predicted from joint inversion, are less than those
323 calculated in zone A, the basement densities range between approximately 2800kgm^{-3} and 2900kgm^{-3}
324 (Figure 6(d)) and the corresponding seismic velocities range between 6.5kms^{-1} and 6.75kms^{-1}
325 (Figure 6(e)).

326 *Zone C - Continental crust*

327 At the eastern end of the profile we interpret continental crust as the crustal basement thickness
328 and both the sediment corrected RDA and RDA_{CT} increase, whilst the continental lithosphere
329 thinning factors decrease to between 0.2 and 0.4. The predicted basement densities range between
330 2800kgm^{-3} and 2855kgm^{-3} and the seismic velocities range between 6.5kms^{-1} and 6.8kms^{-1}. The
331 average basement density for zone C is approximately 2830kgm^{-3}, which is within the range
332 proposed for the density of continental crust (Carlson and Herrick, 1990; Christensen and Mooney,
333 1995; Le Pichon and Sibuet, 1981) and is similar to that used within the initial gravity anomaly
334 inversion (2850kgm^{-3}). Zone C includes the margin necking zone.

335 4. Palaeo-bathymetry of the base Aptian salt deposition from reverse post-
336 breakup thermal subsidence modelling

337 The palaeo-bathymetry of the base Loeme salt (top Aptian) deposition on the Angolan rifted
338 continental margin has been determined using reverse post-breakup subsidence modelling (Kusznir

et al., 1995; Roberts et al., 1998). We have focussed on the CS1-2400 profile, but have also looked at two further profiles to the north, P3 and P7+11 profiles (Contrucci et al., 2004; Moulin et al., 2005). Reverse post-breakup subsidence modelling consists of the sequential flexural isostatic backstripping of the post-breakup sedimentary sequences, decompaction of the remaining sedimentary units and reverse modelling of post-breakup lithosphere thermal subsidence. The magnitude of continental lithosphere stretching factor (β) (McKenzie, 1978) which we predict from gravity anomaly inversion controls the amount of reverse post-breakup thermal subsidence and hence the restored model elevation relative to sea level and the predicted palaeo-bathymetry (Roberts et al., 2009; Roberts et al., 1998).

Flexural backstripping and decompaction has been applied to the CS1-2400 profile (Figure 7(a)) to remove the salt and post-salt sedimentary layers in order to determine the bathymetry corrected for sedimentary loading to base salt (Figure 7(b)). The complex salt movement in this region may appear to be problematic for flexural backstripping. However, within the palaeo-bathymetric restoration we use the base salt as the target surface for backstripping, which allows us to ignore the salt movement, as we flexurally backstrip through the salt to the time of deposition. We are able to disregard the salt movement because as the salt moved the lithosphere would have responded isostatically to compensate.

Flexural backstripping and decompaction gives an incomplete palaeo-bathymetric restoration of base salt; we also need to include reverse post-breakup thermal subsidence. We determine the magnitude of reverse post-breakup thermal subsidence by the continental lithosphere thinning factor ($\gamma=1-1/\beta$) derived from gravity anomaly inversion. Lithosphere thinning factors from gravity inversion are shown in Figure 7(c) assuming a 112Ma rift age for the thermal gravity anomaly correction in the gravity inversion; sensitivities for a normal magmatic solution and a magma-starved solution have been examined. As discussed in previous sections the continental lithosphere thinning factors for a normal magmatic solution are 1.0 at the western end of the CS1-2400 profile; whereas

for a magma-starved solution, the continental lithosphere thinning factors are approximately 0.85. In the central section of the profile, the continental lithosphere thinning factors are between 0.7 and 0.85 for both solutions examined.

Figure 7(d) shows the restored palaeo-bathymetry to base salt, including reverse thermal subsidence modelling, assuming a normal magmatic solution and a breakup age of 112Ma. The proximal base salt restores to just below global sea level with an average bathymetry of approximately 0.2km. In contrast, the distal base salt does not restore to near sea level; restored palaeo-bathymetries for the distal base salt (smoothing through fault controlled topography) are between approximately 0.9km and 2.5km below global sea level. In the deep fault controlled troughs, palaeo-bathymetries for the distal base salt of approximately 4.0km below sea level are predicted.

The restored palaeo-bathymetry to base salt, assuming a magma-starved solution (Figure 7(e)), also shows that the proximal base salt restores to approximately 0.2km below global sea level, whilst the distal base salt again does not. The predicted palaeo-bathymetries of the distal base salt range between approximately 0.9km and 3km below sea level (smoothing through fault controlled topography); in the deep structural troughs the palaeo-bathymetries are greater (approximately 4.5km below sea level).

We believe that the normal magmatic addition solution (Figure 7(d)) is applicable to the oceanic part of the profile whilst the magma-starved solution (Figure 7(e)) is more applicable to the continental end of the profile, with a transitional region in between. In the oceanic domain, water depths at breakup of approximately 2.5km (± 0.2km depending on magmatic solution), consistent with a young oceanic ridge are predicted, for both a normal magmatic and a magma-starved solution.

Rifting on the Angola margin is believed to have commenced in the Neocomian (Teisserenc and Villemin, 1989). For the inner margin, beneath the proximal salt, the main rifting event may have been in the Barremian (Crosby et al., 2011). If a rift age of 130Ma is used to give the lithosphere

388 thermal correction in the gravity inversion and in the reverse post-breakup subsidence modelling,
389 then the proximal base salt restores to approximately 0.6km below global sea-level. There still
390 remains a substantial difference between the restored bathymetry of base proximal and distal salt.

391 As discussed earlier it is possible that our interpretation has overestimated the thickness of the distal
392 salt. We have examined the effect of treating the salt layer as a sedimentary layer within the gravity
393 inversion and the reverse post-breakup subsidence modelling. Reducing the thickness of the salt has
394 a negligible effect on the predicted bathymetry of both proximal and distal salt.

395 An additional sensitivity to the continental lithosphere thinning factors, used to drive reverse
396 thermal subsidence, has been examined along the CS1-2400 profile. A continental lithosphere
397 thinning factor of 1.0 (corresponding to $\beta=\infty$), which gives an upper bound of the restored post-
398 breakup thermal subsidence, has been applied to the entire profile. The predicted bathymetry for
399 the distal base salt remains almost unchanged at between 2km and 3km below global sea level. This
400 implies that, if the distal base salt was deposited at or just below global sea level, it has subsided not
401 only due to post-breakup thermal subsidence and sediment loading.

402 The location of the outer (or more distal) interpreted COB, determined from integrated quantitative
403 analysis, is identified, by the dashed line on Figure 7, in order to examine where the salt is located
404 within the OCT. We believe that the majority of the salt along the CS1-2400 profile is located to the
405 east of the COB on hyper-extended continental crust.

406 In addition to the CS1-2400 profile, we have also applied the reverse post-breakup thermal
407 subsidence modelling to the more northerly P3 and P7+11 profiles (Figure 8). Results are
408 comparable to those predicted for the CS1-2400 profile; with the proximal base salt restoring to
409 approximately sea level whilst the distal base salt restores to between 2km and 3km below global
410 sea level. Predicted thinning factors from gravity inversion, assuming normal magmatic addition, are
411 1.0 at the western end of both P3 and P7+P11 profiles consistent with the presence of oceanic crust.

412 Predicted palaeo-bathymetries for the western end of both profiles are on average 2.85km,
413 consistent with water depths on newly formed oceanic crust. For both profiles, the predicted
414 palaeo-bathymetries for base proximal salt are at or just below global sea level, while the palaeo-
415 bathymetry of base distal salt is between 2km and 3km.

416 # 5. Discussion

417 ## 5.1. Crustal structure and COB location

418 Integrated quantitative analysis using gravity anomaly inversion, RDA analysis, subsidence analysis
419 and joint inversion of deep seismic reflection and gravity data have been used to determine the OCT
420 structure, COB location and magmatic type along the CS1-2400 profile, northern Angolan. Our
421 analysis shows the changes in crustal structure along profile, from which we have interpreted three
422 well defined crustal domains: oceanic crust, hyper-extended continental crust and continental crust
423 (Figure 9(a)). We have also interpreted a transitional region between the hyper-extended
424 continental crust and the start of oceanic crust. Interpretation of our results suggests that at the
425 oceanic end of the profile a normal magmatic solution is applicable, whilst at the continental end of
426 the profile a magma-starved solution is more applicable. Considering the integrated quantitative
427 analysis techniques together has enabled a robust geological interpretation of the OCT along the
428 profile to be made and a more accurate estimate the COB location to be made.

429 Our interpretation of the integrated quantitative analysis results along the CS1-2400 profile is shown
430 in Figure 9(a); our analysis suggests that:

431 (i) Gravity and deep seismic reflection data predict that the earliest oceanic crust is
432 approximately 5km to 7km thick.
433 (ii) RDA analysis shows a slightly positive sediment corrected RDA in the oceanic domain,
434 consistent with the presence of mantle dynamic uplift, which is in agreement with that
435 reported by Crosby & McKenzie (2009).

(iii) Gravity inversion, RDA analysis and subsidence analysis all suggest that both proximal and distal salt is underlain by hyper-extended continental crust, not by oceanic crust.

(iv) Between the oceanic crust and the hyper-extended continental crust domain, we interpret transitional crust, which we believe to be a mix of hyper-extended continual crust and magmatics addition. Our interpretation of this crust is significantly different to the interpretation of serpentinised exhumed mantle from Unternehr et al. (2010).

(v) Gravity anomaly inversion, RDA analysis and subsidence analysis results show that the OCT along CS1-2400 is quite wide, with the distance between the COB and the margin necking zone measuring approximately 180km.

(vi) Joint inversion of deep seismic reflection and gravity data shows a contrast in basement density and seismic velocity between oceanic and continental crustal basement consistent with our domain of transitional crust between the oceanic crust and the hyper-extended crust.

5.2. Palaeo-bathymetry and depositional environment of base Aptian salt

Predicted palaeo-bathymetries have been determined for the base Loeme salt using 2D-flexural backstripping and decompaction, together with reverse modelling of post-breakup thermal subsidence. Continental lithosphere thinning factors derived from gravity anomaly inversion have been used to determine the reverse post-breakup thermal subsidence. For profile CS1-2400, thinning factors, derived from both the normal magmatic and magma-starved gravity inversion solutions assuming a rift age of 112Ma, and used to drive the reverse post-rift thermal subsidence modelling, restore the proximal autochthonous base salt to approximately 0.2km below global sea level at the time of breakup. In contrast, reverse post-breakup subsidence modelling restores the distal base salt to between 2km and 3km below global sea level. Similar palaeo-bathymetries for base salt are also calculated for the more northerly P3 and P7+11 profiles. If we apply a continental lithosphere thinning factor of 1.0 to drive the reverse post-rift thermal subsidence along the full

length of the three profiles (which is unreasonable), the palaeo-bathymetries of base distal salt still do not restore to sea level, demonstrating that it is not possible to generate the subsidence of the base salt by post-rift subsidence alone. The predicted bathymetries at breakup of the first unequivocal oceanic crust are approximately 2.5km as expected for newly formed oceanic crust of normal thickness. Using a rift age of 130Ma for the proximal margin increases the predicted palaeo-bathymetry of base proximal salt to approximately 0.6km below global sea-level, consistent with the analysis of Crosby et al. (2011).

Our preferred interpretation of the palaeo-bathymetric restoration of the distal and proximal base salt is that all the Aptian salt was deposited between 0.2km and 0.6km below global sea level but the distal salt was emplaced during late syn-rift while the continental crust under it was being actively thinned resulting in additional tectonic subsidence. This is consistent with seismic evidence, which shows that the distal base salt is extensionally faulted. This is also in agreement with the observation by Karner and Gambôa (2007) that the rate of subsidence required to generate the accommodation space for the distal salt is too large to be generated by thermal post-breakup subsidence. Crustal basement thicknesses from gravity inversion, RDA and subsidence analysis, summarised in Figure 6, suggest that the distal salt is underlain by hyper-extended continental crust (Figure 9(b)) rather than oceanic crust or exhumed mantle as previously suggested by some authors (e.g. Reston (2010); Unternehr et al. (2010)) . In contrast to the distal salt, the proximal salt formed in a region where crustal thinning had taken place commencing in the Neocomian or Barremian, but had ceased by the upper Aptian, and is consistent with the pre-salt sag sequence under the proximal salt being post-rift (Crosby et al., 2011; Unternehr et al., 2010) Our interpretation requires that the distal salt subsides by syn-rift crustal thinning and post-rift thermal subsidence, whilst the proximal salt subsides by post-rift thermal subsidence alone. Diachronous thinning of the continental crust from inboard to outboard is to be expected from both observation and modelling ,and is consistent with breakup tectonic models proposed by Péron-Pinvidic and Manatschal (2008), Pindell and Kennan (2007), Ranero and Perez-Gussinye (2010) and Brune et al. (2014).

An alternative explanation for the different subsidence styles of proximal and distal salt has been proposed by Karner and Gambôa (2007) who suggest that the sag style subsidence of proximal salt but syn-tectonic style for distal salt are the result of depth-dependent lithosphere stretching and thinning. While depth-dependent lithosphere stretching and thinning has been reported at rifted margins (Davis and Kusznir, 2004; Driscoll and Karner, 1998; Kusznir and Karner, 2007), diachronous rifting and thinning of the Angolan margin lithosphere from inboard to outboard may provide a simpler explanation for the differing subsidence styles of proximal and distal salt.

An alternative interpretation is that the distal salt is para-autochthonous, and it moved down slope to its present position during breakup. If in the distal regions, the salt is para-autochthonous (or allochthonous) this suggests that it was not deposited in deep water and that the salt should not restore to sea level. This interpretation is similar to that advocated in the Gulf of Mexico by Hudec et al. (2013) and Rowan and Vendeville (2006).

An interpretation which is often invoked (e.g. Burke & Sengör (1988), Burke et al. (2003)) to explain the palaeo-bathymetry of the base Aptian salt along the northern Angolan margin is that the distal Aptian salt deposition occurred in confined environmental conditions (e.g. in a Messinian-type basin, isolated from global sea level). Although a structural barrier in the south and north is not dismissed (and is indeed likely), we believe that there is no definite requirement to invoke an isolated ocean basin with local sea level between 2km and 3km below global sea level for the deposition of the Aptian salt on the Angolan rifted margin. Furthermore our analysis suggests that both proximal and distal salt on the Angolan margin are underlain by hyper-extended continental crust, not by oceanic crust. The restored bathymetries of base proximal salt from this study (and also Crosby et al. (2011)) are no more than 0.6km below global sea-level; a deep isolated ocean basin between 2km and 3km deep for the deposition of distal salt would require a substantial difference is the depth of salt deposition level, which we consider to be unlikely. A similar observation has been made by Moulin et al. (2005) and Aslanian et al. (2009). Additional strong arguments against the isolated

basin interpretation are also presented by Pindell et al. (2014) with reference to the Gulf of Mexico; they argue that an isolated basin hypothesis is unlikely as it requires a complicated scenario of inter-related events to occur.

In summary the integrated quantitative analysis predicts the presence of oceanic crust at the western end of the profile; whilst in the centre of the profile, beneath the majority of the Aptian salt we interpret hyper-extended continental crust. We believe that both proximal and distal Aptian salt on the Kwanza margin was deposited at a datum 0.2km to 0.6km below global sea level, but that the distal salt was deposited during late syn-rift while the crust under it was being actively thinned which resulted in additional tectonic subsidence. It is possible that some of the distal salt is para-autochthonous and moved down-slope to its present day position. It is also possible that syn-tectonic (pre-breakup) extension continued post-salt deposition in the distal region.

6. Figure Captions

Figure 1: Data used in the reverse post-breakup thermal subsidence modelling and gravity anomaly inversion for the northern Angolan rifted continental margin. (a) Bathymetry (km) (Amante and Eakins 2009), with the location of profiles CS1-2400, P3 and P7+11 indicated. (b) Satellite derived free air gravity (mgal) (Sandwell and Smith 2009). (c) Deep long-offset seismic reflection depth section (PSDM) for the ION CS1-2400 profile. (d) Seismic velocity model along the P3 profile (Contrucci et al., 2004; Moulin et al., 2005) from seismic refraction data. (e) Seismic velocity model along the P7+11 profile (Contrucci et al., 2004; Moulin et al., 2005) from seismic refraction data.

Figure 2: (a) Crustal cross section along the CS1-2400 profile, showing Moho depth from gravity anomaly inversion, using the calibrated reference Moho depth of 35.5km. (b) Continental lithosphere thinning profile, predicted from gravity anomaly inversion, along the CS1-2400 profile. Sensitivities to a normal magmatic solution and a magma-starved solution have been examined. A normal magmatic solution predicts thinning factors of 1.0 at the western end of the profile, while a magma-starved solution predicts thinning factors of approximately 0.85.

Figure 3: (a) Bathymetry and depth to top basement for the CS1-2400 profile. (b) Comparison of the uncorrected RDA results with the sediment corrected RDA results along the CS1-2400 profile.

Figure 4: (a) Bathymetry and depth to top basement for the CS1-2400 profile. (b) Continental lithosphere thinning factors from subsidence analysis, along the CS1-2400 profile. Sensitivities to a normal magmatic margin, magma-starved solution and a solution for serpentinised mantle are shown.

Figure 5: (a) ION CS1-2400 PSTM deep long offset seismic profile. The horizons for seabed, top basement, Moho predicted from gravity anomaly inversion and picked seismic Moho are indicted. (b) Crustal cross-section along the CS1-2400 profile showing Moho depth from gravity anomaly inversion, and the Moho depth determined from joint inversion; both are in good agreement, with

some variation in magnitude. (c) Lateral variations in basement density along the CS1-2400 profile. The blue dashed line highlights the basement density of 2850kgm^{-3} which is the basement density used within the initial gravity anomaly inversion. Densities range between 2770kgm^{-3} and 2970kgm^{-3}. (d) The corresponding lateral variations in seismic velocity along the CS1-2400 profile.

Figure 6: Summary of the integrated quantitative analysis results for the CS1-2400 profile used to determine OCT structure and COB location. (a) Crustal cross section along CS1-2400 profile, with Moho depth from gravity anomaly inversion. (b) The sediment corrected RDA and the RDA component from variations in crustal basement thickness both have the same general trend along the profile although the magnitudes differ. (c) Comparison of continental lithosphere thinning factors determined using subsidence analysis and gravity anomaly inversion assuming a normal magmatic solution show the same general trend along profile. (d) Smoothed crustal basement densities predicted from the joint inversion of deep seismic and gravity anomaly data. (e) Corresponding seismic velocities predicted from the joint inversion of deep seismic and gravity anomaly data. The dashed lines indicate the interpreted boundaries between the predicted crustal domains.

Figure 7: Flexural backstripping and reverse post-breakup thermal subsidence modelling along the ION CS1-2400 profile. (a) Digitized present day cross section along the CS1-2400 profile; the post-salt sedimentary layer is highlighted in blue; pre-salt sedimentary layer in pink; the salt layer is highlighted in yellow; crust is grey and mantle is red. (b) Sediment corrected bathymetry to base salt calculated from flexural backstripping and decompaction, using a Te of 1.5km. (c) Continental lithosphere thinning factor profile, from gravity anomaly inversion, for normal magmatic and magma-starved solutions. (d) Reverse post-breakup thermal subsidence modelling along the CS1-2400 profile, assuming a normal magmatic solution. (e) Reverse post-breakup thermal subsidence modelling along the CS1-2400 profile, assuming a magma-starved solution.

Figure 8: Flexural backstripping and reverse post-breakup thermal subsidence modelling along the P3 and P7+11 profiles (Contrucci et al., 2004; Moulin et al., 2005). (a) Digitized present day cross section along the P3 profile; (f) Digitized present day cross section along the P7+11 profile; the post-salt sedimentary layers are highlighted in turquoise, orange, green and blue; pre-salt sedimentary layer in pink; the salt layer is highlighted in yellow; crust is grey and mantle is red. (b and g) Sediment corrected bathymetry to base salt calculated from flexural backstripping and decompaction, using a Te of 1.5km. (c and h) Continental lithosphere thinning factors from gravity anomaly inversion for a normal magmatic and a magma-starved solution. (d and i) Reverse post-breakup thermal subsidence modelling along the P3 profile, assuming a normal magmatic solution. (e and j) Reverse post-breakup thermal subsidence modelling along the P3 profile, assuming a magma-starved solution.

Figure 9: (a) Interpretation of the integrated quantitative analysis results along the PSDM CS1-2400 profile. Seabed is shown in blue, top basement in green, Moho from gravity anomaly inversion in black and Moho from the joint inversion is shown in pink. Our interpreted boundaries between the predicted crustal domains are indicated by the dashed lines. (b) Digitized present day cross section along the CS1-2400 profile; location of distal salt and proximal salt and interpreted subsidence history is indicated above.

7. References

Alvey, A., Gaina, C., Kusznir, N. J., and Torsvik, T. H., 2008, Integrated crustal thickness mapping and plate reconstructions for the high Arctic: Earth and Planetary Science Letters, v. 274, no. 3-4, p. 310-321.

Amante, C., and Eakins, B. W., 2009, ETOPO1 1 Arc-Minute Global Relief Model: Procedures, Data Sources and Analysis: NOAA Technical Memorandum NESDIS NGDC-24, p. 19.

Aslanian, D., Moulin, M., Olivet, J.-L., Unternehr, P., Matias, L., Bache, F., Rabineau, M., Nouzé, H., Klingelheofer, F., Contrucci, I., and Labails, C., 2009, Brazilian and African passive margins of the Central Segment of the South Atlantic Ocean: Kinematic constraints: Tectonophysics, v. 468, no. 1–4, p. 98-112.

Birch, F., 1964, Density and composition of mantle and core: Journal of Geophysical Research, v. 69, no. 20, p. 4377-4388.

Brune, S., Heine, C., Pérez-Gussinyé, M., and Sobolev, S. V., 2014, Rift migration explains continental margin asymmetry and crustal hyper-extension: Nat Commun, v. 5.

Burke, K., MacGregor, D. S., and Cameron, N. R., 2003, Africa's petroleum systems: four tectonic 'Aces' in the past 600 million years: Geological Society, London, Special Publications, v. 207, no. 1, p. 21-60.

Burke, K., and Sengör, A. M. C., 1988, Ten metre global sea-level change associated with South Atlantic Aptian salt deposition: Marine Geology, v. 83, no. 1–4, p. 309-312.

Carlson, R. L., and Herrick, C. N., 1990, Densities and porosities in the oceanic crust and their variations with depth and age: Journal of Geophysical Research: Solid Earth, v. 95, no. B6, p. 9153-9170.

Carlson, R. L., and Raskin, G. S., 1984, Density of the ocean crust: Nature, v. 311, no. 5986, p. 555-558.

Chappell, A. R., and Kusznir, N. J., 2008, Three-dimensional gravity inversion for Moho depth at rifted continental margins incorporating a lithosphere thermal gravity anomaly correction: Geophysical Journal International, v. 174, no. 1, p. 1-13.

Christensen, N. I., and Mooney, W. D., 1995, Seismic velocity structure and composition of the continental crust: A global view: Journal of Geophysical Research: Solid Earth, v. 100, no. B6, p. 9761-9788.

Contrucci, I., Matias, L., Moulin, M., Géli, L., Klingelhofer, F., Nouzé, H., Aslanian, D., Olivet, J.-L., Réhault, J.-P., and Sibuet, J.-C., 2004, Deep structure of the West African continental margin (Congo, Zaïre, Angola), between 5°S and 8°S, from reflection/refraction seismics and gravity data: Geophysical Journal International, v. 158, no. 2, p. 529-553.

Cowie, L., 2015, Determination of Ocean Continent Transition Structure, Continent Ocean Boundary Location and Magmatic Type at Rifted Continental Margins [PhD: University of Liverpool, 280 p.

Cowie, L., and Kusznir, N., 2012, Mapping crustal thickness and oceanic lithosphere distribution in the Eastern Mediterranean using gravity inversion: Petroleum Geoscience, v. 18, no. 4, p. 373-380.

Crosby, A. G., and McKenzie, D., 2009, An analysis of young ocean depth, gravity and global residual topography: Geophysical Journal International, v. 178, no. 3, p. 1198-1219.

Crosby, A. G., White, N. J., Edwards, G. R. H., Thompson, M., Corfield, R., and Mackay, L., 2011, Evolution of deep-water rifted margins: Testing depth-dependent extensional models: Tectonics, v. 30, no. 1, p. n/a-n/a.

Davis, M., and Kusznir, N., 2004, Depth Dependant lithospheric Stretching at Rifted Continental Margins, *in* Karner, G. D., Taylor, B., Driscoll, N. W., and Kohlstedt, D. L., eds., Rheology and Deformation of the Lithosphere at Continental Margins, Columbia University Press, p. 408.

Dean, S. M., Minshull, T. A., Whitmarsh, R. B., and Louden, K. E., 2000, Deep structure of the ocean-continent transition in the southern Iberia Abyssal Plain from seismic refraction profiles: The IAM-9 transect at 40°20′N: Journal of Geophysical Research: Solid Earth, v. 105, no. B3, p. 5859-5885.

Discovery 215 Working, G., Minshull, T. A., Dean, S. M., Whitmarsh, R. B., Russell, S. M., Louden, K. E., and Chian, D., 1998, Deep structure in the vicinity of the ocean-continent transition zone under the southern Iberia Abyssal Plain: Geology, v. 26, no. 8, p. 743-746.

Driscoll, N. W., and Karner, G. D., 1998, Lower crustal extension across the Northern Carnarvon basin, Australia: Evidence for an eastward dipping detachment: Journal of Geophysical Research: Solid Earth, v. 103, no. B3, p. 4975-4991.

Fowler, C. M. R., 2006, The Solid Earth: An Introduction to Global Geophysics, Cambridge University Press, 685 p.:

Greenhalgh, E. E., and Kusznir, N. J., 2007, Evidence for thin oceanic crust on the extinct Aegir Ridge, Norwegian Basin, NE Atlantic derived from satellite gravity inversion: Geophysical Research Letters, v. 34, no. 6, p. L06305.

Hudec, M. R., and Jackson, M. P. A., 2007, Terra infirma: Understanding salt tectonics: Earth-Science Reviews, v. 82, no. 1–2, p. 1-28.

Hudec, M. R., Norton, I. O., Jackson, M. P. A., and Peel, F. J., 2013, Jurassic Evolution of the Gulf of Mexico Salt Basin: AAPG Bulletin, v. 97, no. 1, p. 1683 - 1710.

Jackson, M. P. A., Cramez, C., and Fonck, J.-M., 2000, Role of subaerial volcanic rocks and mantle plumes in creation of South Atlantic margins: implications for salt tectonics and source rocks: Marine and Petroleum Geology, v. 17, no. 4, p. 477-498.

Karner, G. D., and Driscoll, N. W., 1999, Tectonic and stratigraphic development of the West African and eastern Brazilian Margins: insights from quantitative basin modelling: Geological Society, London, Special Publications, v. 153, no. 1, p. 11-40.

Karner, G. D., Driscoll, N. W., and Barker, D. H. N., 2003, Syn-rift regional subsidence across the West African continental margin: the role of lower plate ductile extension: Geological Society, London, Special Publications, v. 207, no. 1, p. 105-129.

Karner, G. D., Driscoll, N. W., McGinnis, J. P., Brumbaugh, W. D., and Cameron, N. R., 1997, Tectonic significance of syn-rift sediment packages across the Gabon-Cabinda continental margin: Marine and Petroleum Geology, v. 14, no. (7-8), p. 973-1000.

Karner, G. D., and Gambôa, L. A. P., 2007, Timing and origin of the South Atlantic pre-salt sag basins and their capping evaporites: Geological Society, London, Special Publications, v. 285, no. 1, p. 15-35.

Kusznir, N. J., and Karner, G. D., 2007, Continental lithospheric thinning and breakup in response to upwelling divergent mantle flow: application to the Woodlark, Newfoundland and Iberia margins: Geological Society, London, Special Publications, v. 282, no. 1, p. 389-419.

Kusznir, N. J., Roberts, A. M., and Morley, C. K., 1995, Forward and reverse modelling of rift basin formation: Geological Society, London, Special Publications, v. 80, no. 1, p. 33-56.

Le Pichon, X., and Sibuet, J.-C., 1981, Passive margins: A model of formation: Journal of Geophysical Research: Solid Earth, v. 86, no. B5, p. 3708-3720.

Ludwig, W. J., Nafe, J. E., and C. L. Drake , A. E., 1970, Seismic refraction, in The Sea, Wiley-Interscience, 53-84 p.:

Manatschal, G., Froitzheim, N., Rubenach, M., and Turrin, B. D., 2001, The role of detachment faulting in the formation of an ocean-continent transition: insights from the Iberia Abyssal Plain: Geological Society, London, Special Publications, v. 187, no. 1, p. 405-428.

Manatschal, G., Sutra, E., and Péron-Pinvidic, G., The lesson from the Iberia-Newfoundland rifted margins: how applicable is it to other rifted margins?, *in* Proceedings 2nd Central & North Atlantic Conjugate Margins: Rediscovering the Atlantic, New Insights, New winds for an old sea2010, Volume 2, p. 27 - 37.

McKenzie, D., 1978, Some Remarks on the Development of Sedimentary Basins Earth and Planetary Science Letters, v. 40, p. 25-32.
Moulin, M., 2003, Etude géologique et géophysique des marges continentales passives: exemple du Zaıre et de l'Angola [PhD: University de Bretagne Occidentale, 360 p.
Moulin, M., Aslanian, D., Olivet, J.-L., Contrucci, I., Matias, L., Géli, L., Klingelhoefer, F., Nouzé, H., Réhault, J.-P., and Unternehr, P., 2005, Geological constraints on the evolution of the Angolan margin based on reflection and refraction seismic data (ZaïAngo project): Geophysical Journal International, v. 162, no. 3, p. 793-810.
Müller, R. D., Roest, W. R., Royer, J.-Y., Gahagan, L. M., and Sclater, J. G., 1997, Digital isochrons of the world's ocean floor: Journal of Geophysical Research, v. 102, no. B2, p. 3211-3214.
Müller, R. D., Sdrolias, M., Gaina, C., Steinberger, B., and Heine, C., 2008, Long-Term Sea-Level Fluctuations Driven by Ocean Basin Dynamics: Science, v. 319, no. 5868, p. 1357-1362.
Parker, R. L., 1972, The Rapid Calculation of Potential Anomalies: Geophysical Journal of the Royal Astronomical Society, v. 31, no. 4, p. 447-455.
Parsons, B., and Sclater, J. G., 1977, An Analysis of the Variation of Ocean Floor Bathymetry and Heat Flow with Age: Journal of Geophysical Research, v. 82, no. 5, p. 803-827.
Péron-Pinvidic, G., and Manatschal, G., 2008, The final rifting evolution at deep magma-poor passive margins from Iberia-Newfoundland: a new point of view: International Journal of Earth Sciences, v. 98, no. 7, p. 1581-1597.
Péron-Pinvidic, G., Manatschal, G., Minshull, T. A., and Sawyer, D. S., 2007, Tectonosedimentary evolution of the deep Iberia-Newfoundland margins: Evidence for a complex breakup history: Tectonics, v. 26, no. 2, p. TC2011.
Pindell, J. L., and Kennan, L., 2007, Rift models and the salt-cored marginal wedge in the norhten Gulf of Mexico: implications for dep water paleogene Wilcox deposition and basinwide maturation: Transactions of GCSSEPM 27th Annual Bob F. Perkins Research Conference, p. 146-186.
Ranero, C. R., and Perez-Gussinye, M., 2010, Sequential faulting explains the asymmetry and extension discrepancy of conjugate margins: Nature, v. 468, no. 7321, p. 294-299.
Reston, T. J., 2010, The opening of the central segment of the South Atlantic: symmetry and the extension discrepancy: Petroleum Geoscience, v. 16, no. 3, p. 199-206.
Roberts, A. M., Corfield, R. I., Kusznir, N. J., Matthews, S. J., Hansen, E.-K., and Hooper, R. J., 2009, Mapping palaeostructure and palaeobathymetry along the Norwegian Atlantic continental margin: Møre and Vøring basins: Petroleum Geoscience, v. 15, no. 1, p. 27-43.
Roberts, A. M., Kusznir, N. J., Corfield, R. I., Thompson, M., and Woodfine, R., 2013, Integrated tectonic basin modelling as an aid to understanding deep-water rifted continental margin structure and location: Petroleum Geoscience, v. 19, no. 1, p. 65-88.
Roberts, A. M., Kusznir, N. J., Yielding, G., and Styles, P., 1998, 2D flexural backstripping of extensional basins; the need for a sideways glance: Petroleum Geoscience, v. 4, no. 4, p. 327-338.
Rowan, M. G., and Vendeville, B. C., 2006, Foldbelts with early salt withdrawal and diapirism: Physical model and examples from the northern Gulf of Mexico and the Flinders Ranges, Australia: Marine and Petroleum Geology, v. 23, no. 9–10, p. 871-891.
Sandwell, D. T., and Smith, W. H. F., 2009, Global marine gravity from retracked Geosat and ERS-1 altimetry: Ridge segmentation versus spreading rate: Journal of Geophysical Research, v. 114, no. B1, p. B01411.
Sclater, J. G., and Christie, P. A. F., 1980, Continental stretching: An explanation of the Post-Mid-Cretaceous subsidence of the central North Sea Basin: Journal of Geophysical Research: Solid Earth, v. 85, no. B7, p. 3711-3739.
Stein, C. A., and Stein, S., 1992, A model for the global variation in oceanic depth and heat flow with lithospheric age: Nature, v. 359, no. 6391, p. 123-129.

746 Teisserenc, P., and Villemin, J., 1989, Sedimentary basin of Gabon – geology and oil systems, *in*
747 Edwards, J. D., and Santogrossi, P. A., eds., Divergent / Passive Margin Basins. Memoir of the
748 American Association of Petroleum Geologists, Volume 48.
749 Unternehr, P., Péron-Pinvidic, G., Manatschal, G., and Sutra, E., 2010, Hyper-extended crust in the
750 South Atlantic: in search of a model: Petroleum Geoscience, v. 16, no. 3, p. 207-215.
751 White, R., and McKenzie, D., 1989, Magmatism at Rift Zones: The Generation of Volcanic Continental
752 Margins and Flood Basalts: Journal of Geophysical Research, v. 94, no. B6, p. 7685-7729.
753 Whitmarsh, R. B., and Miles, P. R., 1995, Models of the development of the West Iberia rifted
754 continental margin at 40°30N deduced from surface and deep-tow magnetic anomalies:
755 Journal of Geophysical Research: Solid Earth, v. 100, no. B3, p. 3789-3806.

756

757

758

759

Figure 1

Cowie, Angelo, Kusznir, Manatschal & Horn 2014

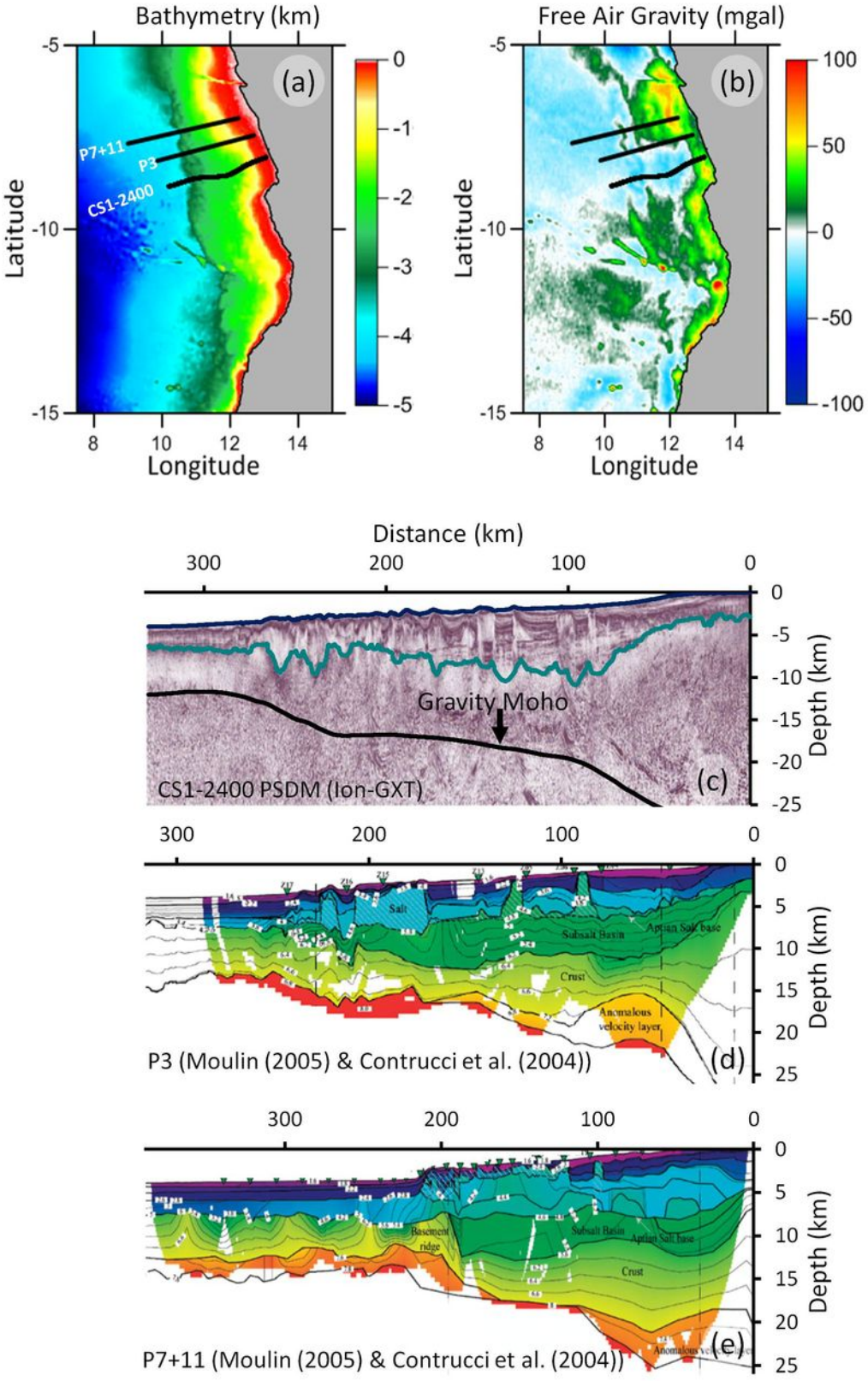

Figure 2

Cowie, Angelo, Kusznir, Manatschal & Horn 2014

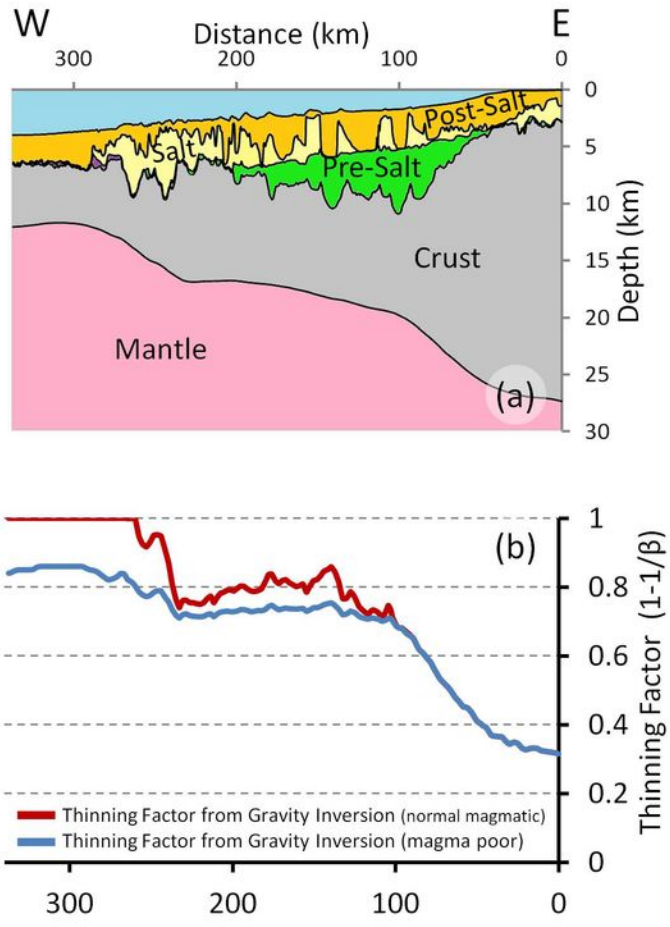

Figure 3

Cowie, Angelo, Kusznir, Manatschal & Horn 2014

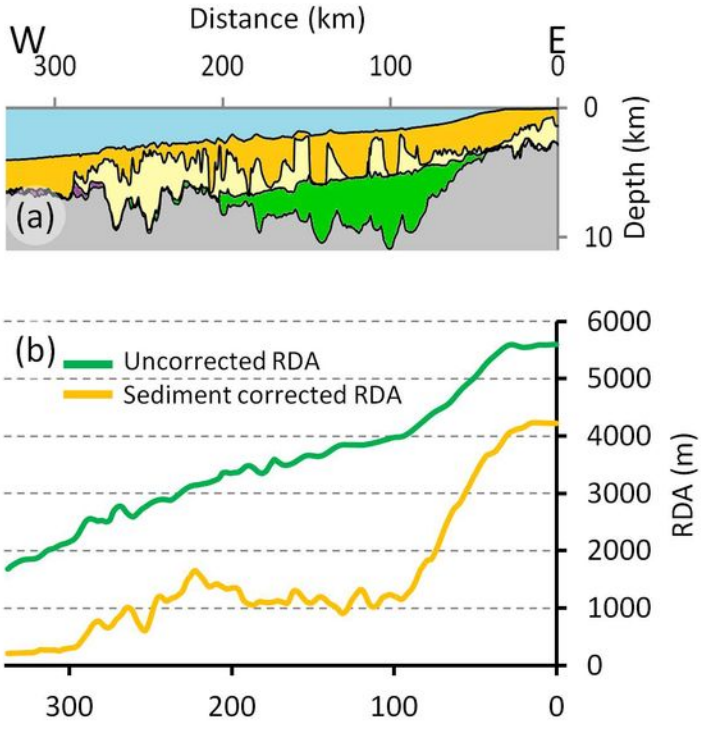

Figure 4

Cowie, Angelo, Kusznir, Manatschal & Horn 2014

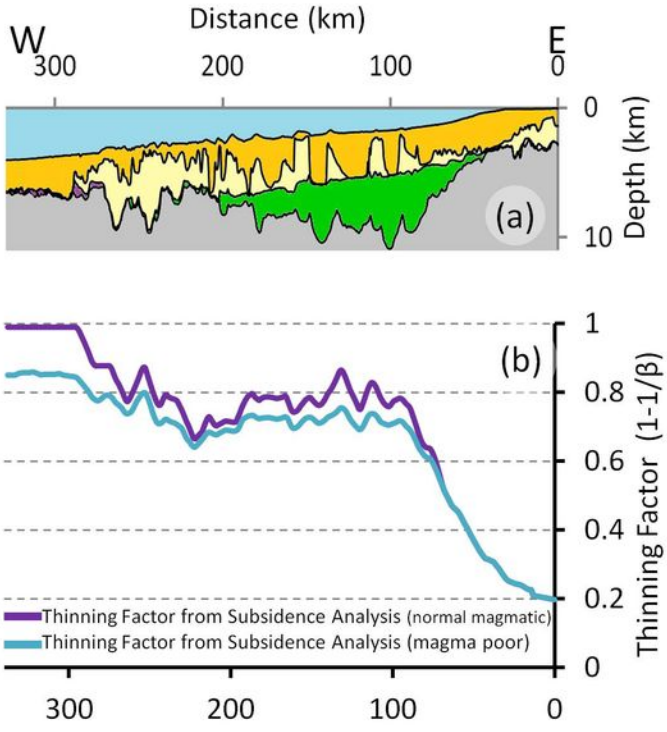

Figure 5

Cowie, Angelo, Kusznir, Manatschal & Horn 2014

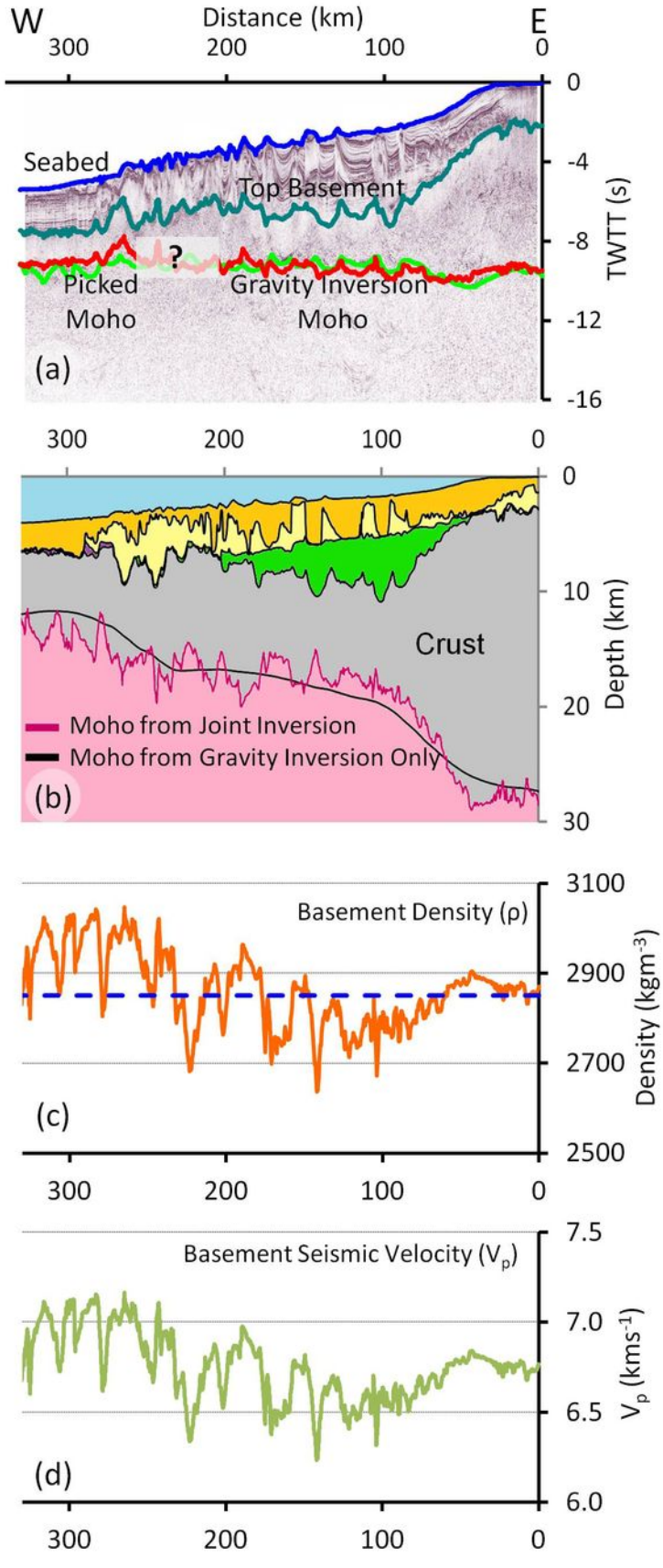

Figure 6

Cowie, Angelo, Kusznir, Manatschal & Horn 2014

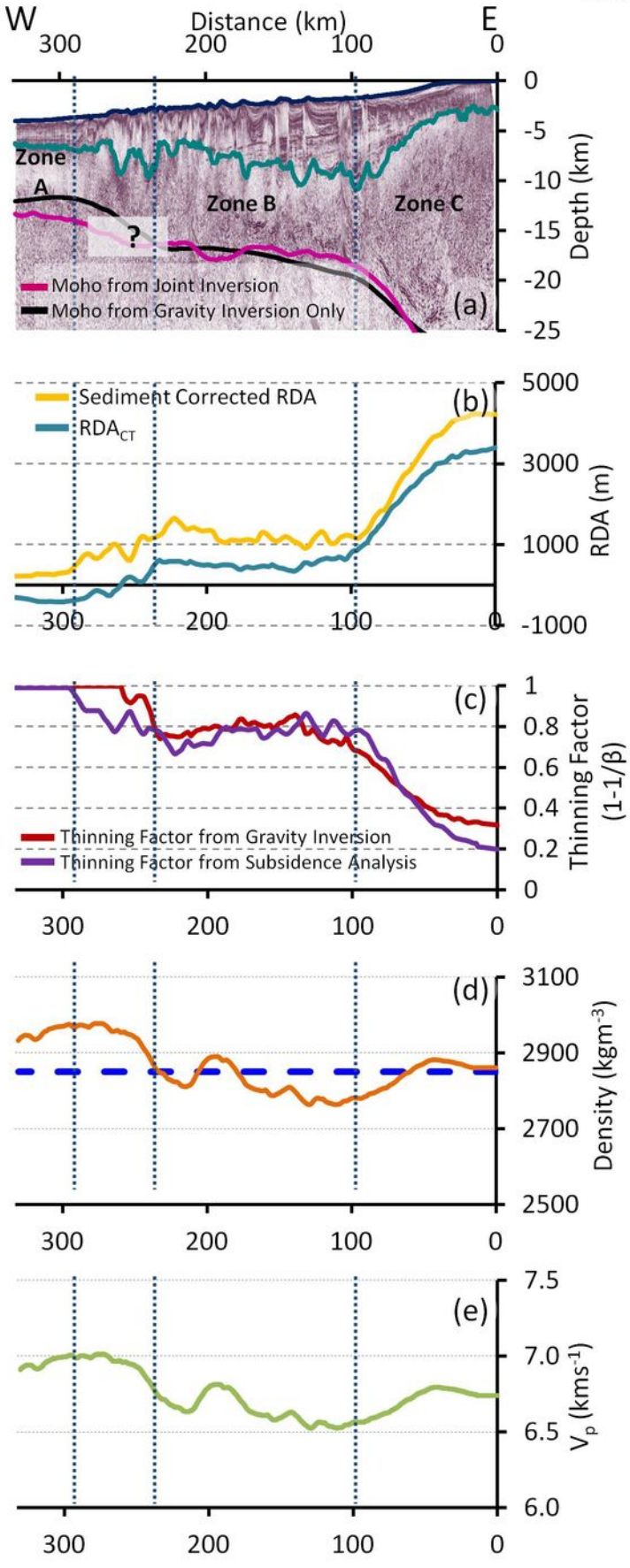

Figure 7

Cowie, Angelo, Kusznir, Manatschal & Horn 2014

ION-GXT CS1-2400 profile:

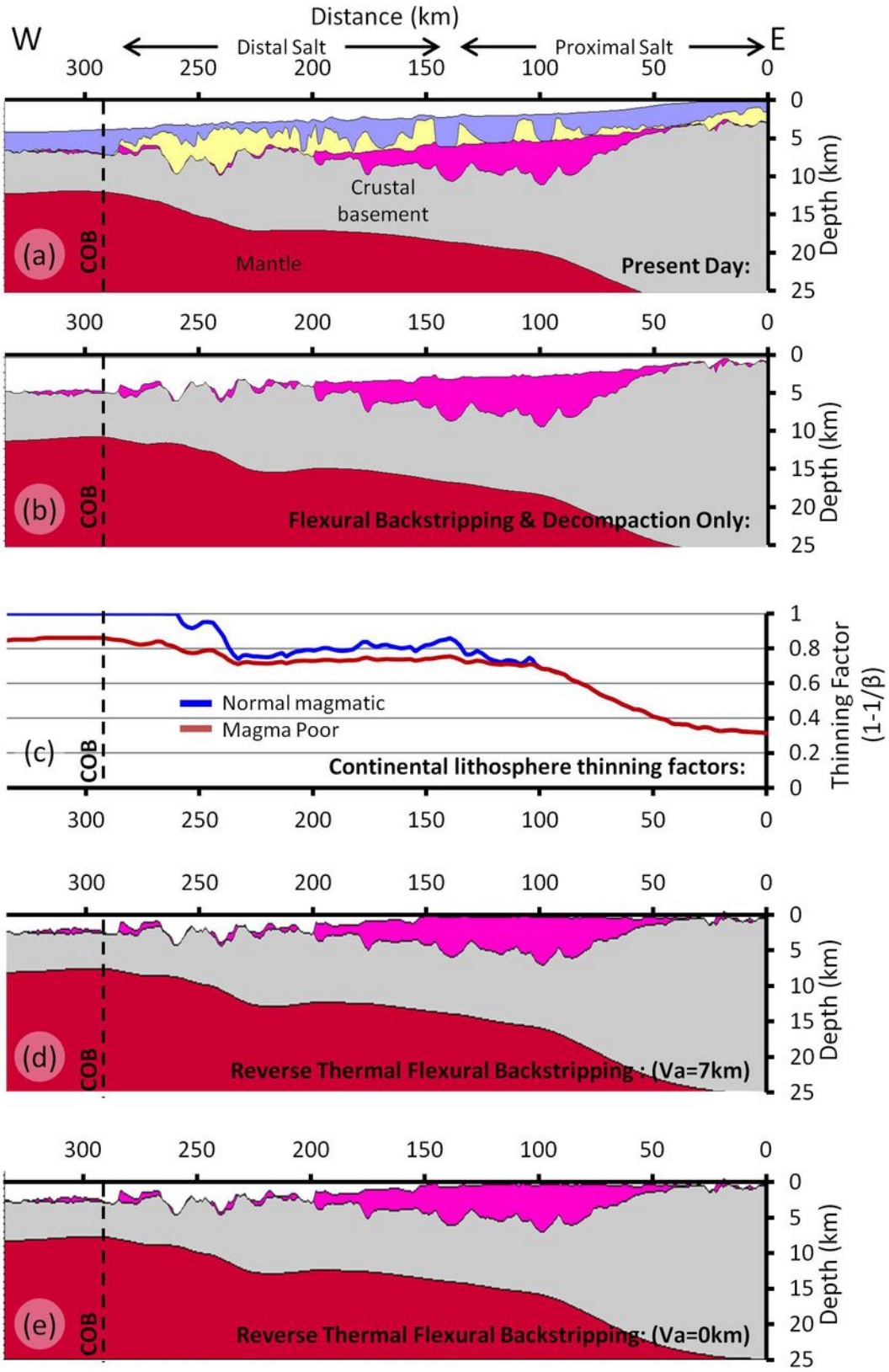

Figure 8

Cowie, Angelo, Kusznir, Manatschal & Horn 2014

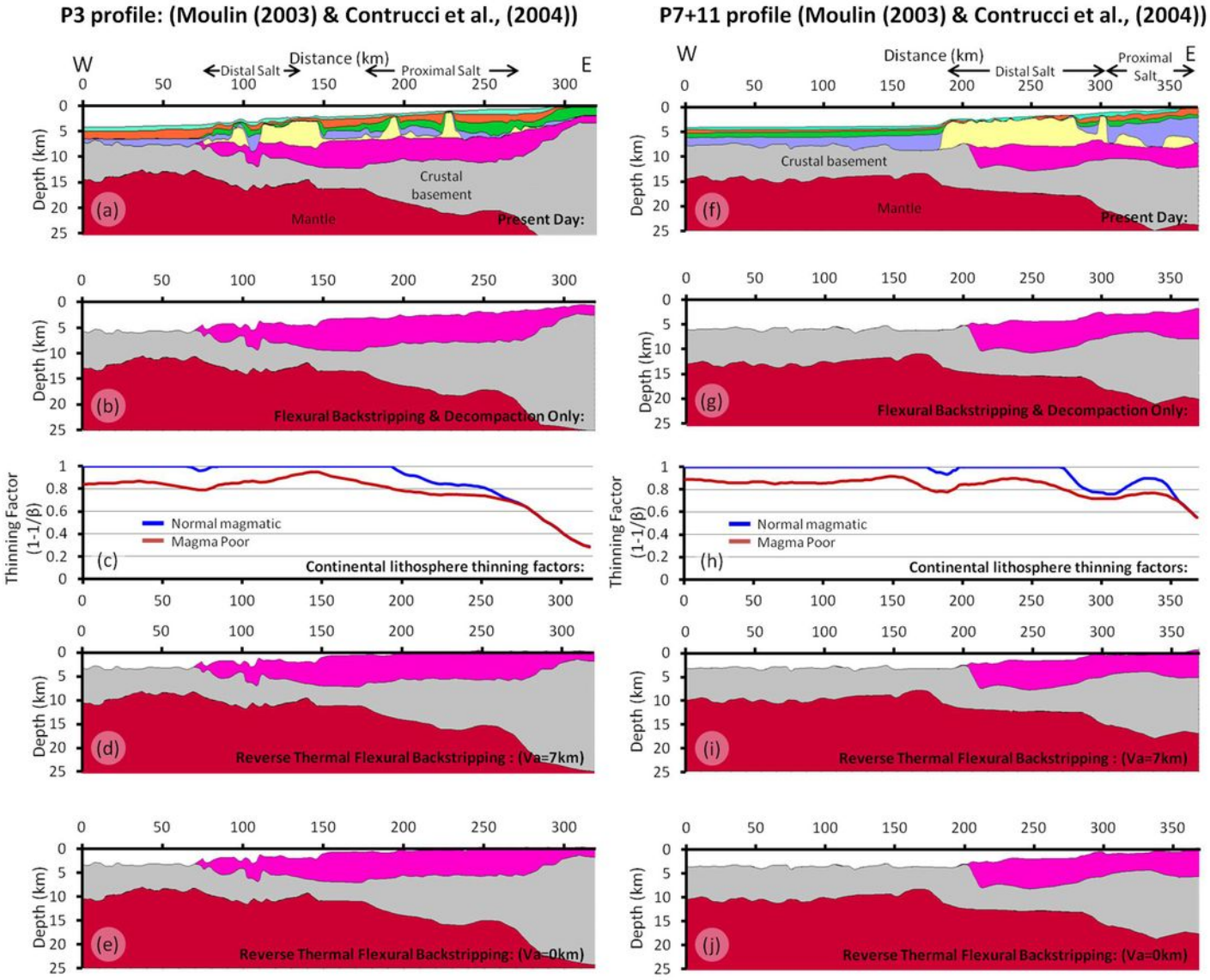

Figure 9

Cowie, Angelo, Kusznir, Manatschal & Horn 2014